J Mater Sci (2007) 42:1228–1237
DOI 10.1007/s10853-006-0079-7

Synthesis of pure tetragonal zirconium oxide with high surface area

M. Rezaei · S. M. Alavi · S. Sahebdelfar · Zi-Feng Yan · H. Teunissen · J. H. Jacobsen · J. Sehested

Received: 23 January 2006 / Accepted: 27 March 2006 / Published online: 23 January 2007

Abstract Zirconium oxide (ZrO_2) with high surface area and high content of the tetragonal polymorph was prepared by precipitation from aqueous solutions under basic conditions in the presence of hexadecyltrimethylammonium bromide as surfactant. The surfactant to zirconium molar ratio, pH of precipitation, aging time and zirconium concentration in aqueous solution were optimized by the Taguchi method. The sample, prepared under optimized conditions had a high surface area of 168 m^2 g^{-1} after calcination at 600 °C for 10 h. Pellets, prepared by pressing this sample and after calcination at 800 °C for 0.5 h had a surface area of 105 m^2 g^{-1}. X-ray diffraction analyses showed that both heat treatments gave pure tetragonal zirconium oxide.

M. Rezaei (✉) · S. M. Alavi
Chemical Engineering Department, Iran University of Science and Technology, Tehran, Iran
e-mail: me_rezaei@yahoo.com

S. Sahebdelfar
Petrochemical Research and Technology Company (NPC-RT), Tehran, Iran

M. Rezaei · Z.-F. Yan (✉)
State Key Laboratory for Heavy Oil Processing, Key Laboratory of Catalysis, CNPC, China University of Petroleum, Dongying 257061, China
e-mail: zfyancat@hdpu.edu.cn

H. Teunissen · J. H. Jacobsen · J. Sehested
Haldor Topsøe A/S, Nymøllevej 55, 2800 Lyngby, Denmark
e-mail: JSS@topsoe.dk

Introduction

Zirconium oxide (Zirconia, ZrO_2) has become one of the industrially most important ceramic materials and also is a potential third-generation catalyst support [1–4]. ZrO_2 has three polymorphs: monoclinic (m-phase, below 1,170 °C), tetragonal (t-phase, between 1,170 °C and 2,370 °C) and cubic (c-phase, above 2,370 °C) [4, 5]. The high temperature cubic and tetragonal phases can be stabilized at room temperature by incorporating dopants in the lattice, e.g. CaO, MgO, Y_2O_3 and CeO_2 [6–8]. The tetragonal phase (t-ZrO_2), has both acidic and basic properties [9] and give the most active catalyst for some catalytic reactions [10]. Another point is that the higher density of tetragonal versus monoclinic ZrO_2 results in higher volume based activity for the tetragonal systems provided that the weight based activities are similar. However, the thermal stability of t-ZrO_2 is crucial since the transition from the tetragonal to the monoclinic phase results in sintering and deactivation of the catalyst. The use of zirconia requires a high specific surface area and suitable pore structure. However, zirconium oxides generally have surface areas of 50 m^2 g^{-1} or less, which is rather low compared with conventional supports such as SiO_2, Al_2O_3 or TiO_2. Higher surface areas are attainable with amorphous zirconia (200–300 m^2 g^{-1}), but this was usually achieved at the expense of much lower thermal stability [11]. Many methods have been explored to get superfine ZrO_2 powders with high surface area, such as the glycothermal process [12], the alcohothermal-SCFD (supercritical fluid drying) process [13, 14], CO_2 supercritical drying [15, 16], the sol–gel method [17, 18] and the solid-state reaction

method [19]. Precipitation by increasing the pH of a zirconium salt solution resulting in a gelatinous, amorphous hydroxide is well known. The composition of this precipitate is not well defined and may be expressed by the general formula $Zr(OH)_xO_{(4-x)/2} \cdot nH_2O$. In most reports, solutions of $ZrOCl_2$, $ZrCl_4$ or zirconyl nitrate are used. The nitrate has the advantage that it is removed rather easy in the calcination stage relative to the chloride [20]. Su et al. [13] reported zirconia precipitation by adding a solution of $ZrOCl_2$ (0.15 mol l^{-1}) to an ammonium hydroxide solution (25 wt.%). The pH of the solution was maintained at 10. The resultant gel was filtered, and then washed with deionized water until no Cl^- was detected. This method produced 16 nm zirconia particles with a specific surface area about 37.8 m^2 g^{-1} and pure monoclinic phase after calcination at 450 °C for 3 h. Zirconia with a well-developed mesoporous structure was obtained by gel-precipitation [21, 22]. The average pore diameter increases from ca. 3.16 nm to 20.6 nm as the calcination temperature was raised from 450 °C to 850 °C. The surface area after calcination at 450 °C for 15 h was 111 m^2 g^{-1}. Chuah et al. [23] prepared zirconium oxide by precipitation from aqueous solutions of zirconium chloride with ammonium hydroxide. The specific surface after calcination at 600 °C for 12 h was 155 m^2 g^{-1} and the ZrO_2 was purely tetragonal. The use of surfactants during the precipitation affords nano crystalline metal oxide with high surface area [24]. In this method there are several parameters, which significantly affect the surface area of the zirconium oxide, such as pH of precipitation, aging time, surfactant to metal molar ratio and zirconium to water molar ratio. The Taguchi method, which is common in the design of industrial experiments, may be used for optimization of the precipitation [25, 26]. The utilization of this technique for catalyst optimization as well as in various sol–gel processes have been reported [27–29]. If interactions between design parameters are neglected and error analysis is performed using some approximate techniques, the Taguchi method requires a significantly smaller number of experiments compared with other statistical techniques [30]. Although some information is lost due to the two mentioned approximations, it is still worth choosing this approach at the initial stage of material design, considering the time consuming nature of the precipitation experiments. In this work, the Taguchi method was used to optimize the preparation conditions for synthesis of zirconium oxide with high surface area and high content of the tetragonal polymorph.

Experimental

Materials

The starting materials were $ZrO(NO_3)_2 \cdot xH_2O$ (x ca. 6; Aldrich), $ZrOCl_2 \cdot 8H_2O$ (Aldrich), hexadecyltrimethylammonium bromide (CTAB; Fluka) and ammonium hydroxide (25 wt.%; Fluka).

Zirconia preparation

In a typical preparation, aqueous ammonia (25 wt.%) was added dropwise at room temperature to an aqueous solution containing zirconium precursor and hexadecyltrimethylammonium bromide under rapid stirring. After precipitation, the slurry was stirred for another 30 min and then heated at 80 °C for a certain time under continuous stirring. The mixture then was cooled to room temperature, filtered and washed, first with deionized water and finally with acetone for an effective removal of the surfactant. The final product was dried at 100 °C for 24 h under flowing air and calcined at different conditions. A diagram of the preparation is shown in Fig. 1.

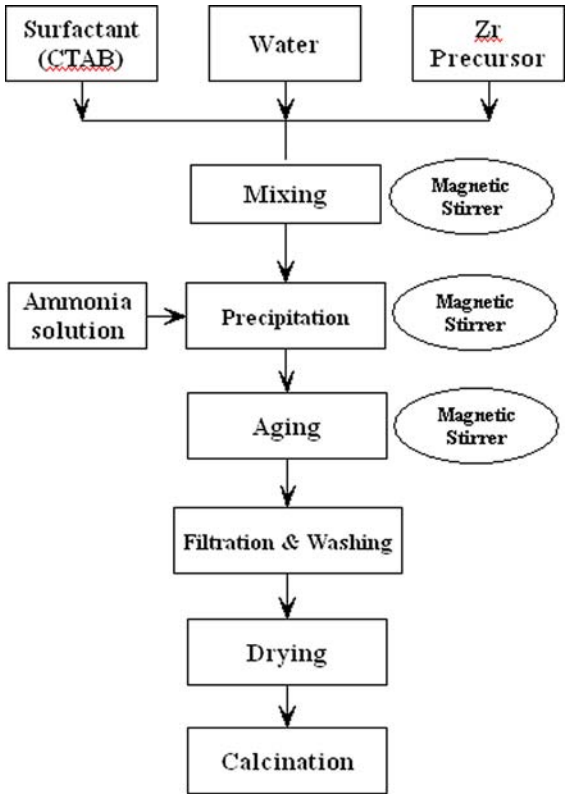

Fig. 1 The preparation of zirconium oxide

For determining the effect of zirconium precursors on the tetragonal weight fraction and the specific surface area, two precursors were used; $ZrO(NO_3)_2 \cdot xH_2O$ and $ZrOCl_2 \cdot 8H_2O$. In these experiments surfactant/Zr molar ratio, Zr molarity, pH and aging time were chosen as 0.8, 0.00983 mol l^{-1}, 11 and 24 h, respectively. After the zirconium precursor had been chosen, the surfactant to zirconium molar ratio, pH of precipitation, aging time and zirconium molarity were considered as the most important parameters for optimization of the precipitation conditions. Three levels of each parameter were used as shown in Table 1.

A L_9 orthogonal array as given in Table 2 was used in experimental design. This design requires nine experiments with four parameters at three levels. Although this design does not have sufficient ''degrees of freedom'' to study ''interactions'' and ''error estimation'' in four-parameter systems, it was chosen since it requires the minimum possible number of experiments. Deriving interactions and error are possible only if a larger orthogonal array is used. This would increase the number of experiments significantly and diminish the advantage of the Taguchi method.

Characterization

The surface areas (BET) were determined by nitrogen adsorption at –196 °C using an Autosorb-1C (Quantachrome,USA) apparatus. The pore size distribution was calculated from the desorption branch of the isotherm by the Barrett, Joyner and Halenda (BJH) method. The XRD pattern were recorded on an X-ray diffractometer (Philips-PW-1840) using a CuK_α monochromatized radiation source and a Ni filter in the range $2\theta = 10–70°$. The relative amounts of tetragonal and monoclinic ZrO_2 present in samples and the crystallite sizes were estimated as described elsewhere [13]. Thermogravimetric (TG) and differential thermal analysis (DTA) were carried out in a Netzsch STA 409 system in a static air atmosphere at a heating rate of 10 °C per minute. Infrared spectra were recorded on a NEXus fourier transform infrared (FTIR) spectrophotometer using KBr pellets containing 1% weight sample in KBr. TEM investigations were performed with Philips CM200 FEG UltraTwin operated at 200 kV. Images were recorded with a Gatan model 794 CCD-camera. Inductively coupled plasma atomic emission spectroscopy (ICP-AES) was used to determine Si content in selected samples using a Shimadzu (Japan) ICPV-1000 apparatus. The samples were dissolved for 10 h in a mixture of HF (46 wt.%) and HCl (36 wt.%) aqueous solutions at 150 °C and diluted with a boric acid (6 wt.%) aqueous solution.

Table 1 Parameters and their experimental levels

Parameter	Level 1	Level 2	Level 3
(A) Surfactant/Zr mol. ratio	0.8	0.5	0.2
(B) pH	11	10	9
(C) Aging time (h)	24	12	6
(D) Zr molarity (mM)	0.983	1.46	2.434

Table 2 L_9 orthogonal array used

Experiment No.	Parameters levels			
	A	B	C	D
1	1	1	1	1
2	1	2	2	2
3	1	3	3	3
4	2	1	2	3
5	2	2	3	1
6	2	3	1	2
7	3	1	3	2
8	3	2	1	3
9	3	3	2	1

Results and discussion

Properties of zirconia samples prepared by precipitation

First, ZrO_2 samples prepared using $ZrO(NO_3)_2 \cdot xH_2O$ and $ZrOCl_2 \cdot 8H_2O$ were calcined at different conditions and characterized by nitrogen adsorption and XRD. Data regarding the precipitation and characterization are given in Table 3.

The specific surface areas of the samples Z-1/Z-3 and Z-2/Z-4, respectively were similar, so the zirconium precursor does not have a large effect on the product specific surface area. With increasing the calcination temperature up to 800 °C, the abundance of the monoclinic phase increased and sintering occurred, resulting in loss of surface area and increase of crystalline size. Because the removal of Cl^- from the precipitate was cumbersome since numerous washing steps were necessary before a $AgNO_3$ solution based Cl^- test was negative, the nitrate salt was used in the following experiments.

Figure 2 shows the IR spectra of the Z-1 sample after drying (curve a) and after calcination at 600 °C for 10 h (curve b). The bands in the regions of 1630 cm^{-1} and 2800–2900 cm^{-1} are attributed to the

Table 3 Properties of ZrO_2 samples prepared with different precursors

Sample	Zr Precursor	Calcination conditions	Tetragonal (wt.%)	Crystallite size (nm)			S_{BET} ($m^2\ g^{-1}$)
				t(101)	t(002)	m($\bar{1}$11)	
Z-1	$ZrO(NO_3)_2 \cdot xH_2O$	600 °C/10 h	88	7.5	6	5.5	123
Z-2	$ZrO(NO_3)_2 \cdot xH_2O$	800 °C/0.5 h	70	10.5	8	8.5	68
Z-3	$ZrOCl_2 \cdot 8H_2O$	600 °C/10 h	100	8.2	6.4	–	117
Z-4	$ZrOCl_2 \cdot 8H_2O$	800 °C/0.5 h	88	11.2	7.9	9.9	65.9

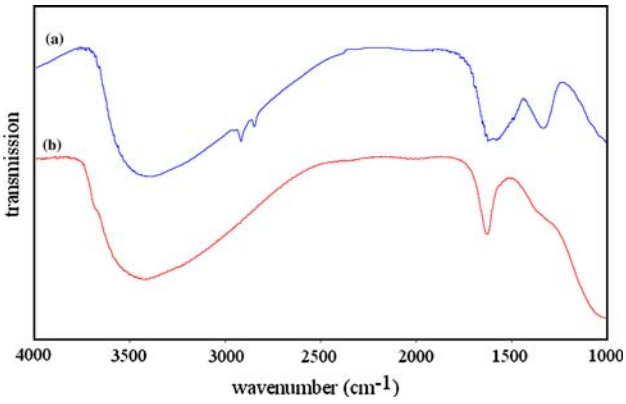

Fig. 2 The FT-IR spectrum for the Z-1, (a) after drying at 100 °C, (b) after calcination at 600 °C for 10 h

hydroxyl group and small amount of CTAB, respectively. Curve b in Fig. 2 also indicates that the CTAB is fully removed by calcination.

The TGA and DTA curves of sample Z-1 are shown in Fig. 3. The DTA curve, presents four major peaks; in which, two are endothermic and the others are exothermic. The first endothermic peak appears at low temperature about 100 °C which corresponds to the elimination of residual water and the second one at about 300 °C is due to the removal of surface hydroxyl groups of the zirconia. Simultaneously, the first exothermic peak at 400 °C is attributed to the oxidation of organic residues and the second one at 570 °C, usually called ''glow exotherm'', is attributed to the crystallization of amorphous zirconia. Simultaneously, the TG curve, is leveled off at about 600 °C, meaning that the organic residues have been removed completely and it also confirmed the FTIR results.

Optimization of precipitation preparation

For optimization of the surface area and the content of the tetragonal polymorph, nine samples were prepared. A Taguchi design of L_9 orthogonal array was used to investigate the factors, such as surfactant/Zr ratio, pH, aging time and Zr molarity (Table 2). The resulting experimental conditions are given in Table 4. All the prepared samples were calcined at 600 °C for 10 h. The tetragonal weight percents obtained from XRD and the BET areas are also given in Table 4. Both the tetragonal weight percent and the surface area varied significantly with the preparation conditions. The variation in the tetragonal percent varied more than a factor of two while the surface area varied by a factor of two. These variations are encouraging as they indicate that it may be possible to optimize the

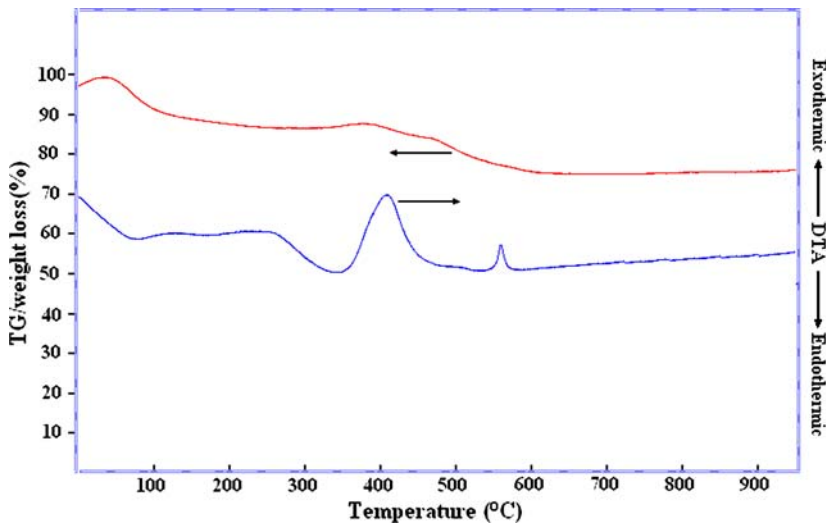

Fig. 3 DTA/TGA curves of the Z-1

Table 4 Experimental conditions and the percent of tetragonal phase and BET area

Exp.	Sample	Surfactant/Zr molar ratio	pH	Aging time (h)	Zr Molarity (mM)	BET area (m^2 g^{-1})	Tetragonal (wt.%)
1	Z-1	0.8	11	24	0.983	123	88
2	Z-5	0.8	10	12	1.460	100.2	79
3	Z-6	0.8	9	6	2.434	61.7	36
4	Z-7	0.5	11	12	2.434	123	91
5	Z-8	0.5	10	6	0.983	79.9	46
6	Z-9	0.5	9	24	1.460	112	89
7	Z-10	0.2	11	6	1.460	86.1	57
8	Z-11	0.2	10	24	2.434	85.2	80
9	Z-12	0.2	9	12	0.983	85.6	63

precipitation conditions to prepare the pure tetragonal ZrO_2 with high surface area.

For a maximization problem, the Taguchi defines a signal-to-noise ratio, which can be calculated from the following equation.

$$\eta = -10\log\left(\frac{1}{n}\sum_{i=1}^{n}\frac{1}{y_i^2}\right) \quad (1)$$

In this equation η is defined as the ''signal/noise ratio'', and y is the response parameter, which is weight percent of tetragonal phase or specific surface area. n is the number of measurements in each experiment which is equal to 1 in this case. In fact, the Taguchi method uses signal-to-noise ratios as response variables. According to Eq. 1, maximizing η is equivalent to maximizing y. The η values corresponding to the weight percent of the tetragonal phase and BET area in each experiment are presented in Table 5. According to Taguchi method, the parameter levels leading to the maximum tetragonal weight percent and specific surface can be found by using the results given in Table 5.

Justification of this argument lies in the properties of the L_9 orthogonal array. Assuming no interaction, the effects of parameter (i) on η can be found by comparing the average responses (Mij) obtained at different levels (j) of that parameter. For example, average response for the tetragonal weight percent of pH at level 1 (pH = 11) is obtained from the sum of the values of $\eta_{\text{tetragonal phase}}$ from experiments 1, 4 and 7 since pH = 11 are used in these experiments (see Table 3):

$$M_{\text{pH=11}} = \frac{\eta_1 + \eta_4 + \eta_7}{3} = \frac{38.88 + 39.18 + 35.11}{3} = 37.22.$$

Similar calculations give $M_{\text{pH = 10}} = 36.42$, $M_{\text{pH = 9}} = 35.36$ indicating that level 1 (pH = 11) of the pH parameter should be chosen to maximize η and therefore the tetragonal weight percent since it has the highest average response. The average responses for all parameters corresponding to the tetragonal weight percent and the specific surface area are given in Table 6.

The so-called main effects plot for the means of signal-to-noise ratio for the tetragonal weight percent is shown in Fig. 4.

Main effects plots show how each factor specifically affects the response. In principle a main effect is present when different levels of a factor affect the characteristic differently. In general the slope of the line is proportional to the extent of the effect while a horizontal line means no effect. By comparing the slopes of the lines, we can estimate the relative magnitude of the effects. For these experiments we

Table 5 $\eta_{\text{tetragonal phase}}$ and $\eta_{\text{surface area}}$ for the nine experiments

Exp.	Sample	Tetragonal phase (wt.%)	$\eta_{\text{tetragonal phase}}$	Specific surface area (m^2 g^{-1})	$\eta_{\text{surface area}}$
1	Z-1	88	38.88	123	41.79
2	Z-5	79	37.95	100.2	40.01
3	Z-6	36	31.12	61.7	35.80
4	Z-7	91	39.18	123	41.79
5	Z-8	46	33.25	79.9	38.05
6	Z-9	89	38.98	112	40.98
7	Z-10	57	35.11	86.1	38.70
8	Z-11	80	38.06	85.2	38.60
9	Z-12	63	35.98	85.6	38.64

Table 6 Response table for means

Level	CTAB/Zr[a]	CTAB/Zr[b]	pH[a]	pH[b]	Aging time[a]	Aging time[b]	Zr molarity[a]	Zr molarity[b]
1	35.98	39.20	37.72	40.76	38.64	40.46	36.12	38.73
2	37.14	40.27	36.42	38.89	37.70	40.15	37.35	39.90
3	36.38	38.65	35.36	38.47	33.16	37.51	36.04	39.49

[a] Corresponding to the tetragonal weight percent

[b] Corresponding to the specific surface area

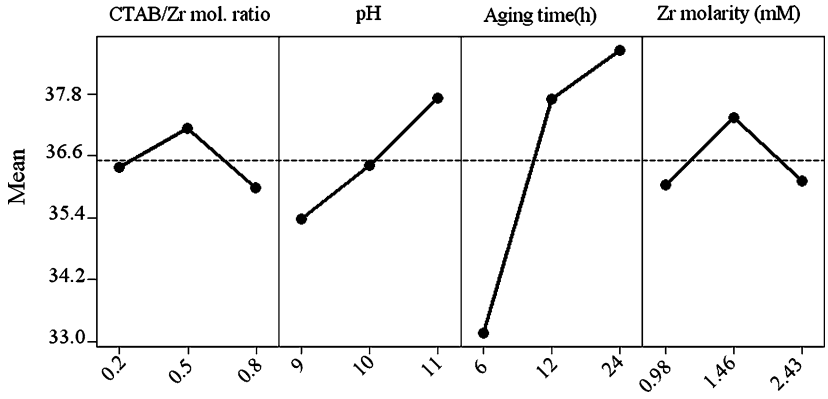

Fig. 4 The main effects plot for the signal-to-noise ratio

can see the pH and aging time have the highest effect on the signal-to-noise ratio. The results indicated that level 2 of surfactant to zirconium molar ratio and Zr molarity and level 1 of pH and aging time will positively influence the weight percent of tetragonal phase and also the specific surface area.

To test this hypothesis, a new zirconium oxide (experiment 10) was prepared using a surfactant to zirconium molar ratio 0.5, pH 11, 24 h aging time and a Zr concentration of 0.001460 mol l^{-1}. The BET analyses of this sample at different calcination conditions are given in Table 7. As it can be seen the BET analysis of Z-16 (calcined at 600 °C for 10 h) showed a specific surface area of 168 m^2 g^{-1} which is a significant improvement.

The XRD pattern, Fig. 5, showed that this sample (Z-16) is pure tetragonal ZrO_2. The crystallite sizes of the sample at different calcination conditions are also given in Table 7. The XRD pattern, Fig. 5, showed that the Z-16 sample is actually pure tetragonal ZrO_2. The crystallite sizes of the Z-16 sample at different calcination conditions are also given in Table 7. The XRD patterns, Fig. 5, illustrated that the samples, calcined at 250, 350 and 450 °C were amorphous and had a high specific surface area (Table 7). While increasing the calcination temperature up to 700 °C, the specific surface area obviously decreases, but the zirconia was still in pure tetragonal phase (Fig. 5).

To determine the effect of the surfactant on the specific surface area and crystallite phase of the zirconia, one sample (Z-18) was prepared under the optimized conditions but without surfactant. The BET analysis of Z-18 (calcined at 600 °C for 10 h) showed a specific surface area of 102 m^2 g^{-1} which is smaller than that of Z-16. It demonstrates that the addition of surfactant during the precipitation has a positive effect

Table 7 Structural properties of the samples

Sample	Calcination conditions	Tetragonal (wt.%)	Crystallite size (nm)					S_{BET} (m^2 g^{-1})
			t(101)	t(110)	t(112)	t(211)	t(202)	
Z-13	200°C/5 h	Amorphous	–	–	–	–	–	410
Z-14	350°C/5 h	Amorphous	–	–	–	–	–	330
Z-15	450°C/5 h	Amorphous	–	–	–	–	–	285
Z-16	600°C/10 h	100	7.2	5.7	5.7	4.7	7.5	168
Z-17	700°C/5 h	100	7.6	6.3	6.1	6	7	127
Z-18	600°C/10 h	100	8.9	10.1	9.3	9.9	6	102

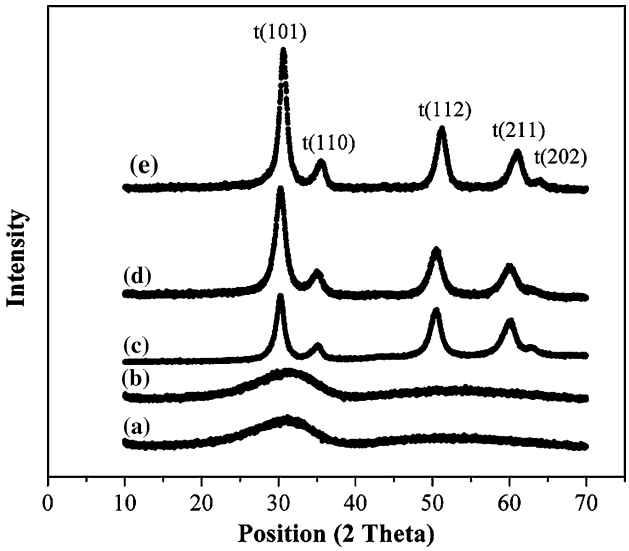

Fig. 5 XRD patterns for the (a) Z-14, (b) Z-15, (c) Z-16, (d) Z-17 and (e) Z-18

on the specific surface area of the sample. The XRD pattern, Fig. 5, also showed that this sample is pure tetragonal ZrO_2, but the crystallite sizes for this sample are bigger than for Z-16 (Table 7).

The pore size distribution and N_2 adsorption/desorption isotherms were determined for Z-16 and Z-18 and the results are plotted in Fig. 6. It is seen that both samples are mesoporous, but the pore size of the Z-16 is smaller than that of Z-18. The nitrogen adsorption/desorption isotherms can be classified as a type IV isotherm, typical of mesoporous materials. According to IUPAC classification, the hysteresis loop is type H2 indicating a complex mesoporous structure.

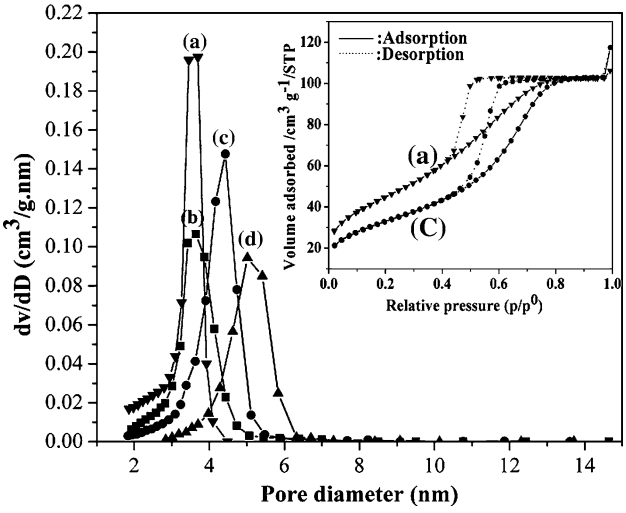

Fig. 6 Pore size distribution and N_2 adsorption/desorption isotherms of (a) Z-16, (b) Z-19, (c) Z-18, (d) Z-20

This type of hysteresis is characteristic of solids consisting of particles crossed by nearly cylindrical channels or made by aggregates (consolidated) or agglomerates (unconsolidated) of spherical particles. In this case the pores have nonuniform size or shape (type H2).

The pore size distributions were also determined for Z-19 and Z-20 which were obtained by pressing Z-16 and Z-18 powder to pellets followed by calcination at 800 °C for 30 min. The pore size distributions are also plotted in Fig. 6. This figure illustrates that the aggregated particles grow and the mesoporosity is increased by increasing the calcination temperature. The comparison of the pore size distributions for Z-19 and Z-20 indicates that the zirconia sample prepared with addition of surfactant has higher thermal stability than the sample without addition of surfactant. The pores of the Z-20 collapsed to a larger extent than those of Z-19 after treatment at 800 °C. The pore volume data for different samples are shown in Table 8.

The XRD patterns and the crystallite sizes for Z-19 and Z-20 are shown in Fig. 7 and Table 9, respectively. The XRD pattern illustrated that the Z-19 pellets were pure tetragonal ZrO_2. The crystallite sizes of Z-19 and Z-16 (zirconium oxide calcined at 600 °C for 10 h) were similar. These results revealed that the tetragonal phase is stable towards higher temperatures. Of interest is that the tetragonal phase was stabilized at room temperature without addition of any dopants. For Z-20 part of tetragonal phase was transformed to the monoclinic phase by increasing the calcination temperature up to 800 °C. Comparison of the crystallite sizes for the Z-19 and Z-20 also indicated that the sample prepared without surfactant shows stronger sintering resulting in bigger crystallite sizes and lower specific surface area.

The TEM analysis (Fig. 8) showed that the zirconia prepared in the presence of surfactant (Z-16 and Z-19) have similar morphology. As it can be seen, particles are closely sintered together and most of the particles have a slightly irregular, rounded shape. The particle sizes in Z-16 are from 4 nm to 10 nm in diameter, while the particle sizes in Z-19 are bigger (from 6 nm to 15 nm).

Thermal stability of t-phase zirconia sample

The thermodynamically most stable ZrO_2 phase at room temperature is the m-phase. Probably, the small size of the ZrO_2 crystallites, leads to the thermal stabilization of t-phase [31, 32]. Garvie suggested that difference in the surface energy between the tetragonal and monoclinic phases could cause the tetragonal

Table 8 The surface area and pore structure of zirconia prepared with surfactant and without surfactant

Sample	Synthesis conditions	Calcination conditions	BET area (m^2 g^{-1})	Pore volume (cm^3 g^{-1})	Pore diameter (nm)
Z-16	With surfactant	600 °C/10 h	168	0.164	3.34
Z-18	Without surfactant	600 °C/10 h	102	0.181	4.65
Z-19	With surfactant	600 °C/10 h–800 °C/0.5 h	105	0.176	4.04
Z-20	Without surfactant	600 °C/10 h–800 °C/0.5 h	54	0.133	5.31

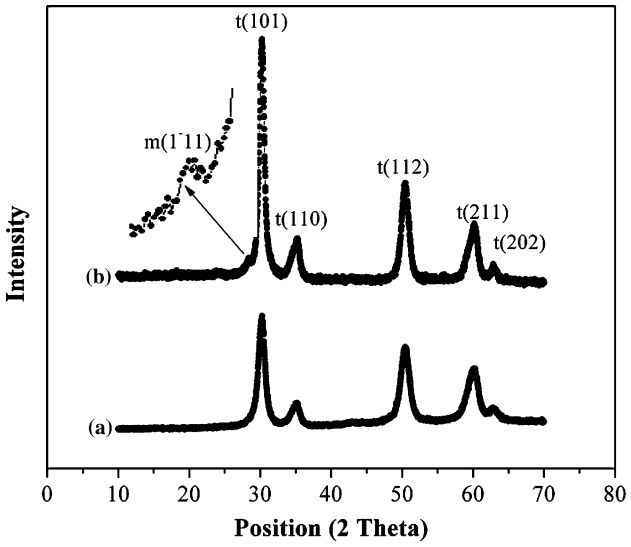

Fig. 7 XRD patterns for the (a) Z-19 and (b) Z-20

Table 9 Structural properties of the Z-19 and Z-20

Sample	Tetragonal (wt.%)	Crystallite size (nm)				
		t(101)	t(110)	t(112)	t(211)	t(202)
Z-19	100	8.5	6	6.6	5.4	7.8
Z-20	71	31.8	14	20.7	5.3	5.5

phase to be thermodynamically stable for very small crystals [33, 34].

The thermodynamic stability of a phase is determined by its total free energy, which is determined by the bulk free energy, but also affected by the surface and strain energy. In case of crystallites with high surface to volume ratio, the surface free energy may become decisive rather than the bulk term in determining the phase stability. The tetragonal phase has lower surface free energy than the monoclinic phase, but has a higher bulk free energy than the monoclinic phase [34]. If we assume spherical isolated ZrO_2 nanocrystals, which have a uniform surface free energy and neglect strain energy, the critical crystallite size (D_c) for transformation at a given temperature can be defined by the following equations given by Garvie [34].

$$D_c = [-6(\gamma_t - \gamma_m)]/[q(1 - T/T_b)], \quad (2)$$

where γ_t and γ_m are surface free energies for the tetragonal and the monoclinic phases, q is the heat of the phase transformation per mole of an infinite crystal, T_b is the transformation temperature of an infinite large crystal and D_c is the critical crystallite size. Substituting $\gamma_t = 0.77$ J m^{-2}, $\gamma_m = 1.13$ J m^{-2}, $q = 2.82 \times 10^8$ J m^{-3}, $T = 298$ K and $T_b = 1{,}448$ K [33, 34], the critical crystal size (D_c) for the mono-

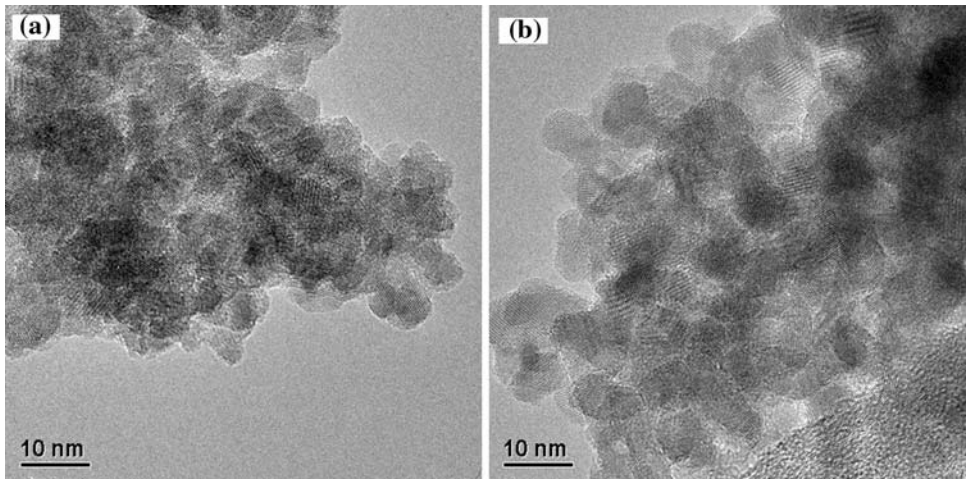

Fig. 8 TEM pictures of the (a) Z-16 and (b) Z-19

clinic-to-tetragonal phase transformation, at room temperature, is calculated to be 9.6 nm.

It is, however, noted that the ZrO_2 nanoparticles, synthesized under the optimized conditions, are not single, spherical isolated ZrO_2 nanocrystals, Fig. 8. As a result, the surface free energies of the ZrO_2 nanoparticles are modified. Moreover, by increasing the calcination temperature, the ZrO_2 nanoparticle size within the aggregates increases, Fig. 8 and Table 9, which suggests the existence of coherency between the ZrO_2 nanocrystallites within the aggregates. Hence, if we assume that the tetragonal ZrO_2 nanoparticles within the aggregates are similar to the coherent precipitates and tend to transform into noncoherent monoclinic particles, then the modified surface free energy values, γ_t and γ_m, can be taken as 0.22 J m^{-2} and 1.46 J m^{-2} for coherent-tetragonal and noncoherent-monoclinic nanocrystallites, respectively [34]. Substituting these modified surface free energy values in Eq. 2, the critical crystal size of 33.2 nm is calculated for the tetragonal phase stabilization within an aggregate. It appears that the critical crystallite size increases from 9.6 nm to 33.2 nm when the single, isolated ZrO_2 nanocrystals become elements of an aggregated particle.

So for the samples, prepared under the optimized conditions the tetragonal phase could be stable, since their crystallite sizes are below the critical crystallite sizes of 33.2 nm. It is also apparent that the equilibrium transformation temperature is only significantly altered for crystals with diameter below 50 nm, Fig. 9. Due to the small crystallite sizes of the ZrO_2 as-prepared here, the tetragonal phase could be effectively stable at low temperature.

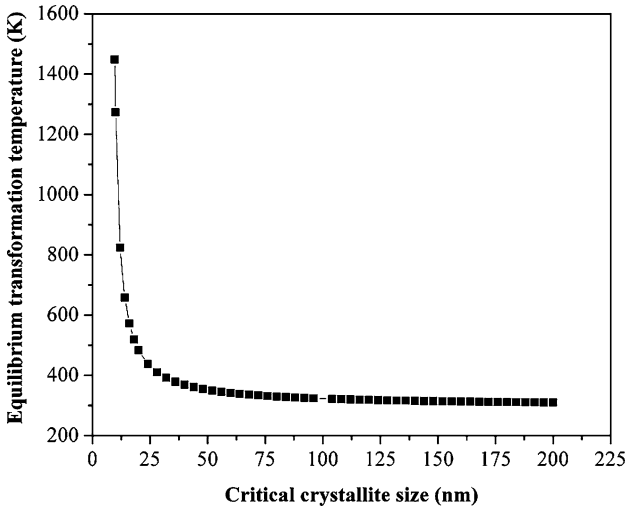

Fig. 9 Equilibrium transformation temperature via the critical crystallite size

Dissolved silica effect

It is well known that the silica component of a glass container can dissolve in an alkaline solution and the dissolution rate increases with an increase in the pH of the solution at pH > 8. Both the dissolution rate and the solubility of silica increase with increasing temperature and pH value [35]. In the case of borosilicate glass such as Pyrex, silica species also dissolve in an alkaline solution, but the dissolution rate is low [36]. Yin and Xu [37] investigated the preparation of ZrO_2 by precipitation and ageing under basic conditions using ordinary glassware. They observed excessive dissolution of Si from the glass container and incorporation into the hydrous zirconia and found that the final surface area of the ZrO_2 was proportional to its Si content. They found a silica content of 5 wt.% in the zirconia prepared at pH of 11.5, a digestion time of 72 h and NH_4OH as precipitation agent and a surface area of about 308 and 174 m^2 g^{-1} after calcination at 600 °C and 800 °C for 5 h. This sample showed an amorphous phase even after calcination at 600 °C for 5 h. The silica contents for Z-16 (0.61 wt.%) and Z-18 (0.73 wt.%) were determined in order to establish the effect of silica on the specific surface area of the optimized sample. The observed Si contents were lower than those obtained by Yin and Xu. It means that the effect of surfactant is much higher than the effect of dissolved silica on the specific surface area, although the presence of silica can considerably enhance the specific surface area.

Mechanism of surfactant effect

A hydrous oxide may exchange either cations or anions, depending on the pH of the medium. Hydrous zirconium oxide effectively incorporates cationic surfactants at a pH well above its isoelectric point [38]. The isoelectric point of hydrous zirconium oxide in aqueous solution is about 6.7. In accordance with this feature the following equilibrium can be expressed for ZrO_2.

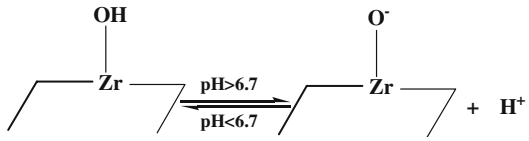

Scheme 1

When the pH of the medium is higher than the pH of the isoelectric point, the equilibrium shifts to the right with a negative charge on the surface and incorporation of cationic surfactant takes place. With increasing pH during precipitation, the interaction

between the cationic surfactant and hydrous zirconia increases and leads to increased surfactant incorporation. At lower pH values, the degree of incorporation of the surfactant is lower, owing to the presence of fewer surface OH groups available for exchange, resulting in a decreasing surface area. The extent of the interaction between the surfactant and hydrous zirconia will presumably increase by increasing the reaction time. This might explain the influence of the pH and aging time on the surface area of zirconia. As well as these surfactants can be added to the pore liquid to reduce the interfacial energy and thereby decrease the surface tension of water contained in the pores. As the hydrous zirconium oxide shrinks, the tension in the pores increases, causing pores to collapse. Surfactant can act by reducing the interfacial energy and decreasing the capillary stress, which has a beneficial effect on pore structure stability.

Conclusions

Pure tetragonal zirconia with a surface area of 168 $m^2 g^{-1}$ after calcination at 600 °C for 10 h has been prepared by an optimization of the precipitation process by the Taguchi method of experimental design. The optimization of the precipitation method indicated that the pH during precipitation and aging time has the largest effects on the specific surface area and the tetragonal weight percent, because the approach we used for synthesis of zirconium oxide with high surface area exploits the interaction of the mixture of hydrous oxides with cationic surfactants under basic conditions. The stabilization of tetragonal phase in the prepared samples can be explained by nano-size effect, which affects the crystallite phase composition and stabilizes tetragonal phase at room temperature. The result of an XRD analysis of an optimized ZrO_2 sample calcined at 800 °C revealed that the tetragonal crystalline phase is relative stable towards higher temperatures even though one third of the surface area is lost during the calcination.

Acknowledgements M. Rezaei takes this opportunity to thank the supports of Haldor Topsøe A/S and Petrochemical Research & Technology Company (NPC-RT).

References

1. Tai CY, Hsiao BY, Chiu HY (2004) Colloids Surf A Physicochem Eng Aspects 237:105
2. Ma T, Huang Y, Yang J, He J, Zhao L (2004) Mater Design 25:515
3. Lee MH, Tai CY, Lu CH (1999) J Eur Ceramic Soc 19:2593
4. Chraska T, King AH, Berndt CC (2000) Mater Sci Eng A 286:169
5. Luo TY, Liang TX, Li CS (2004) Mater Sci Eng A366:206
6. Ray JC, Saha CR, Pramanik P (2002) J Eur Ceramic Soc 22:851
7. Peshev P, Stambolova I, Vassilev S, Stefanov P, Blaskov V, Starbova K, Starbov N (2003) Mater Sci Eng B 97:106
8. Sekulic A, Furic K, Stubicar M (1997) J Mol Struct 410–411:275
9. Yamaguchi T (1994) Catal Today 20:199
10. Centini G, Cerrato G, Angelo SD, Finardi U, Giamello E, Morterra C, Perathorner S (1996) Catal Today 27:265
11. Cao Y, Hu JC, Hong ZS, Deng JF, Fan KN (2002) Catal Lett 81(1–2):107
12. Kongwudthiti S, Praserthdam P, Silveston P, Inouse M (2003) Ceramics Int 29:807
13. Su C, Li J, He D, Cheng Z, Zhu Q (2000) Appl Catal A 202:81
14. Sun Q, Zhang Y, Deng J, Chen S, Wu D (1997) Appl Catal A 152:L165
15. Mrowiec-Bialon J, Pajak L, Jarzebski AB, Lachowski AI, Malinowski JJ (1998) J Non-Crystal Solids 225:115
16. Stocker C, Baiker A (1998) J Non-Crystal Solids 223:165
17. Wang JA, Valenzuela MA, Salmones J, Vázquez A, Garcia-Ruiz A, Bokhimi X (2001) Catal Today 68:21
18. Aguilar DH, Torres-Gonzalez LC, Torres-Martinez LM, Lopez T, Quintana P (2000) J Solid State Chem 158:349
19. Liu XM, Lu GQ, Yan ZF (2004) J Phys Chem B 108:15523
20. Ramamurthi SD, Xu Z, Payne DA (1990) J Am Ceram Soc 73:2760
21. Mercera PDL, Van Ommen JG, Doesburg EBM, Burggraaf AJ, Ross JRH (1990) Appl Catal 57:127
22. Mercera PDL, Van Ommen JG, Doesburg EBM, Burggraaf AJ, Ross JRH (1991) Appl Catal 78:79
23. Chuah GK, Jaenicke S, Cheong SA, Chan KS (1996) Appl Catal A 145:267
24. Hudson MJ, Knowles JA (1996) J Mater Chem 6:89
25. Taguchi G (1986) Introduction to quality engineering, Asian productivity organization. Distributed by American Suppliers Institute Inc., Dearborn, MI
26. Phadke MS (1989) In: Quality engineering using robust design. Prentice Hall, Englewood Cliffs, NJ
27. Dawson EA, Barnes PA (1992) Appl Catal A 90:217
28. Sheth A, Trembath K (2002) J Mater Process Technol 123:167
29. Yang DW, Hung KM, Hsieh CS (2002) Mater Sci Eng A 333:123
30. Montgomery DC (2001) In: Design and analysis of experiments. Wiley, NewYork
31. Skandan G, Foster CM, Frase H, Ali MN, Parker JC, Hahn H (1992) Nanostruct Mater 1:313
32. Garvie RC, Goss MF (1986) J Mater Sci 21:1253
33. Garvie RC (1965) J Phys Chem 69:1298
34. Garvie RC (1978) J Phys Chem 82:218
35. Wijnen PWJ, Beelen TPM, De Haan JW, Rummens CPJ, Van De Ven LJM, Van Santen RA (1989) J Non-Crystal Solids 85:109
36. Perera G, Doremus RH (1991) J Am Ceram Soc 74:1554
37. Yin SF, Xu BQ (2003) Chemphyschem 3:277
38. Hudson MJ, Knowles JA (1996) J Mater Chem 6:89